Guided ion-beam studies of the reactions of Co_n^+ (n=2–20) with O_2: Cobalt cluster-oxide and -dioxide bond energies

Fuyi Liu, Feng-Xia Li, and P. B. Armentrout[a)]

Department of Chemistry, University of Utah, Salt Lake City, Utah 84112

(Received 27 May 2005; accepted 20 June 2005; published online 12 August 2005)

The kinetic-energy dependence for the reactions of Co_n^+ (n=2–20) with O_2 is measured as a function of kinetic energy over a range of 0 to 10 eV in a guided ion-beam tandem mass spectrometer. A variety of Co_m^+, Co_mO^+, and $Co_mO_2^+$ ($m \leqslant n$) product ions is observed, with the dioxide cluster ions dominating the products for all larger clusters. Reaction efficiencies of Co_n^+ cations with O_2 are near unity for all but the dimer. Bond dissociation energies for both cobalt cluster oxides and dioxides are derived from threshold analysis of the energy dependence of the endothermic reactions using several different methods. These values show little dependence on cluster size for clusters larger than three atoms. The trends in this thermochemistry and the stabilities of oxygenated cobalt clusters are discussed. The bond energies of Co_n^+–O for larger clusters are found to be very close to the value for desorption of atomic oxygen from bulk-phase cobalt. Rate constants for O_2 chemisorption on the cationic clusters are compared with results from previous work on cationic, anionic, and neutral cobalt clusters. © *2005 American Institute of Physics*. [DOI: 10.1063/1.1998836]

I. INTRODUCTION

Transition metals, as well as their oxides and alloys, are a subject of considerable interest because of their industrial importance in catalysis, corrosion, and ferromagnetic properties. For example, cobalt is known to be an important catalytic metal in many industrial processes,[1] including Fischer-Tropsch synthesis, in which larger hydrocarbons are produced from synthesis gases (CO and H_2).[2,3] Cobalt oxides, usually with some other metal oxides, are mainly used as hydrotreating and desulfhurization catalysts for oil and gas in the petrochemical industry.[4] Cobalt-based alloys are often utilized as they are wear resistant, corrosion resistant, and heat resistant.[4] Therefore, understanding the mechanisms and energetics of the oxidation processes of transition metals is of some technological value, as well as being of fundamental interest. Studying the oxidation process with gas-phase transition-metal clusters can provide quantitative data concerning the elementary steps that make up the complicated surface processes and thus help elucidate surface science at a molecular level. In this regard, the reactions of Fe,[5] Cr,[6] V,[7] and Ni (Ref. 8) cluster cations with O_2, as well as the reactions of Fe (Ref. 9) and Cr (Ref. 10) clusters with CO_2, have been investigated by our group. In this paper, we extend these studies to examine the reactions of cobalt cluster cations, Co_n^+ (n=2–20), with oxygen.

The gas-phase reactions of cobalt clusters with O_2 have been reported by several groups. Jacobson and Freiser[11] studied the reaction of cobalt dimer and trimer cations with oxygen at thermal energies by using Fourier-transform ion cyclotron resonance (FTICR) mass spectrometry. Freas *et al.*[12] investigated the reactions of cobalt cluster cations with O_2 and collision-induced dissociation (CID) of cobalt oxides in a chemical ionization/fast atom bombardment source. Three different ion product pathways were observed: oxygen deficient products, $Co(CoO)_n^+$; oxygen equivalent products, $(CoO)_n^+$; and to a much lesser extent metal deficient products, $O(CoO)_n^+$. They attribute this behavior to the electropositivity of the cobalt atom, which can accommodate the positive charge. Guo *et al.*[13] examined the size dependence and kinetics of gas-phase reactions of Co_n^+ (n=2–9) with O_2 at thermal energies using a selected ion drift tube with laser vaporization source. They determined the bimolecular reaction-rate constants for the primary reactions, generally formation of $Co_{n-1}O_2^+$+Co (n=4–9). In previous work in our laboratories, Hales and Armentrout[14] measured the kinetic-energy dependence of the reaction of Co_2^+ with dioxygen using guided ion-beam tandem mass spectrometry.

The reactions of neutral and anionic cobalt clusters with O_2 have also been reported. Andersson *et al.*[15] investigated the reactivity of neutral cobalt clusters (n=10–55) with O_2 using two reaction cells under near single-collision conditions. They measured the reaction probability for adsorption of the first and second O_2 molecules using a statistical model. The reactivity of cobalt anion clusters, Co_n^- (n=2–8), toward O_2 was reported by Kapiloff and Ervin[16] using a flow tube reactor. The oxygen-rich anion cluster products are formed rapidly through "etching" -type process, in contrast with the case of cation clusters that yield cobalt-rich oxide cation clusters.[12,13] In addition, Pramann *et al.*[17] have examined anionic cobalt cluster oxides, $Co_nO_m^-$ (n=4–20 and m=0–2), using photoelectron spectroscopy. Recently, neutral oxygenated cobalt species have been studied using infrared spectrometry[18,19] and characterized by density-

a)Electronic mail: armentrout@chem.utah

functional theory calculations.[18–21] Theoretical studies of cobalt monoxide neutral, cation, and anion have also been reported.[22]

In the present work, cobalt cluster cations, Co_n^+ ($n=2-20$), previously examined using collision-induced dissociation with Xe (Ref. 23) and reacted with D_2,[24] are reacted with oxygen. In contrast to the flow reactor studies that are limited to thermal reactions, the kinetic-energy dependence of these reactions over a wide range is studied here using guided ion-beam mass spectrometry. Our reactivity results at thermal energies should reproduce the flow tube data; however, by analyzing the kinetic-energy dependences of these processes, we are able to obtain quantitative data regarding the thermodynamics of the oxidation reactions. The trends in this information are discussed in some detail and compared with bulk-phase thermochemistry. This study is a continuation of our efforts to provide quantitative measurements of the thermodynamics and reactivities of transition-metal clusters, which have shown interesting variations with cluster size.[25–28]

II. EXPERIMENTAL SECTION

A. Instrumentation

The experimental apparatus and techniques in this study have been described in detail elsewhere,[29] and only a brief description is given here. Cluster cations are formed by laser vaporization of a cobalt rod housed in an aluminum source block.[30,31] The output (511 and 578 nm) of an Oxford ACL 35 copper vapor laser operating at 7 kHz is tightly focused onto a continuously translating and rotating cobalt rod to expose fresh surface to the laser. The optimum pulse energy for cobalt cluster ion production ranges between 3 and 4 mJ/pulse. The vaporized material is entrained in a continuous flow [$(5-6)\times10^3$ SCCM (Standard cubic centimeter per minute)] of He passing over the ablation surface. The helium is passed through a liquid-N_2-cooled molecular sieve trap to remove impurities. Frequent collisions and rapid mixing lead to the formation of thermalized clusters as they travel down a 2-mm-diameter$\times$63-mm-long condensation tube. This seeded helium flow then undergoes a mild supersonic expansion and passes through a skimmer in field-free conditions. Previous studies have indicated that the clusters are not internally excited and likely to be near room temperature,[23,24,29] although direct measurements of the internal temperatures of the clusters are not possible.

Positively charged ions pass through two differentially pumped regions and are accelerated and focused into a 60° magnetic sector momentum analyzer. The mass-selected ions are decelerated and injected into a rf octopole ion guide[32,33] that extends through a reaction cell. The octopole beam guide is biased with dc and rf voltages. The former allows accurate control of the translational energy of the incoming ions, whereas the latter establishes a radial potential that efficiently traps the parent and product ions that travel through the octopole. The pressure of O_2 neutral reactant gas in the reaction cell is kept relatively low to reduce the probability of multiple collisions with the ions. To test this, all studies were conducted at two pressures of O_2, ~0.2 and ~0.4 mTorr. The product and reactant ions drift to the end of the octopole, where they are extracted and injected into a quadrupole mass filter for mass analysis. Ion intensities are measured with a Daly detector[34] coupled with standard pulse counting techniques. Reactant ion intensities ranged from 1×10^5 to 8×10^5 ions/s. Observed product intensities are converted to absolute reaction cross sections as discussed in detail elsewhere.[33] Absolute errors in the cross sections are on the order of ±30%. Kinetic energies in the laboratory frame are converted to center-of-mass (CM) energies using the stationary target approximation, $E(\mathrm{CM})=E(\mathrm{lab})m/(m+M)$, where m and M are the masses of the neutral and ionic reactants, respectively. The data at the lowest energies are corrected for truncation of the ion-beam energy distribution.[33]

Results for each reaction system were repeated several times to ensure their reproducibility. CID experiments with Xe were performed on all cluster ions to ensure their identity and the absence of any excessive internal excitation. In all instances, CID thresholds are consistent with those previously reported.[23] The absolute zero in the kinetic energy of the ions and their energy distributions (0.8–1.8 eV, gradually increasing with cluster size) were measured using the octopole as a retarding energy analyzer.[33] The error associated with the zero of the absolute energy scale is 0.05 eV in the laboratory frame.

B. Threshold analysis

The energy dependences of cross sections for endothermic processes in the threshold region are analyzed using methods detailed previously.[35–37] Briefly, the threshold region is modeled using Eq. (1),

$$\sigma(E)=(N\sigma_0/E)\sum_i g_i\int_{E_0-E_i}^{E}[1-e^{-k(E^*)\tau}](E-\varepsilon)^{N-1}d(\varepsilon), \tag{1}$$

where σ_0 is an energy-independent scaling parameter, N is an adjustable parameter, E is the relative kinetic energy, and E_0 is the threshold for reaction at 0 K. The model includes the average vibrational and rotational energies of cluster ions at 300 K, which are evaluated from the respective cluster frequencies and rotational constants by summing over the rovibrational states having energies E_i and relative populations g_i, where $\Sigma g_i=1$. For metal clusters, it has been shown that lifetime effects become increasingly important as the size of the cluster increases.[38] This is because metal clusters have many low-frequency vibrational modes such that energy randomization into cluster internal modes results in a reduced probability of observing dissociation within our experimental time window of $\sim10^{-4}$ s, i.e., the lifetime of the transient intermediate can exceed the experimental time available for reaction. This results in a delayed onset of the observed threshold, a kinetic shift of the experimental threshold towards energies higher than the thermochemical endothermicity. Thus, an important component of the modeling of these reactions is to include the effect of the lifetime of the reaction, as estimated using statistical Rice-Ramsperger-Kassel-Marcus (RRKM) theory,[39–41] as discussed in detail

previously.[42] This is achieved using $k(E^*)$, the unimolecular rate constant for reaction; τ, the experimental time for dissociation ($\sim 10^{-4}$ s); ε, the energy deposited in the complex by the collision; and E^*, the internal energy of the energized molecule (EM) after the collision, i.e., $E^* = \varepsilon + E_i$. The unimolecular rate constant $k(E^*)$ is given as $sN(E^* - E_0)/h\rho(E^*)$, where s is the reaction degeneracy, $N(E^* - E_0)$ is the sum of rovibrational states of the transition state (TS) at an energy $E^* - E_0$, h is Planck's constant, and $\rho(E^*)$ is the density of states of the EM at the available energy of E^*. The model cross section, Eq. (1), is also convoluted with the kinetic-energy distributions of the ion and neutral reactants before comparison to the experimental data.[33]

The choice of the TS and its molecular constants parallels those of our previous work[5] and places the TS at the point where the last atom (Co for all $Co_mO_2^+$ and $Co_{n-1}O^+$ products and O for the Co_nO^+ products) is lost from the oxygenated cluster. The transition state is assumed to be loose, having molecular constants similar to the dissociated products.[42] The implementation of the RRKM theory in the present work requires the vibrational frequencies of the oxygenated clusters, the reaction degeneracy, and rotational constants for the bare metal and oxygenated clusters, which are chosen in accord with the procedures outlined previously.[5] The $3n-6$ vibrations associated with the bare metal cluster are calculated by using an elastic cluster model suggested by Shvartsburg *et al.*[43] In this study, the parameters used are the Debye frequency for bulk cobalt, $\nu_D(\infty)=280$ cm^{-1}, the bulk maximum longitudinal frequency, $\nu_{L,\max}=301$ cm^{-1}, and the ratio of the longitudinal to the transverse phonon velocity, $c_L/c_T=1.81$, which are estimated from the average values of bulk nickel[44,45] and bulk iron,[45–47] respectively. The cluster-oxygen vibrational frequencies of 454 cm^{-1} (symmetric stretch), 435 cm^{-1} (asymmetric stretch), and 401 cm^{-1} (bend) are estimated from the average values of the vibrational frequencies for analogous oxygenated iron and nickel clusters.[5,8] Although these procedures may be oversimplified, the magnitudes of the errors associated with these estimates of frequencies were evaluated by scaling all frequencies by ±50%, which produces differences in the thresholds that are less than 0.04 eV.

III. RESULTS

Guided ion-beam studies for the reactions of atomic Co^+ and diatomic Co_2^+ with oxygen have been reported previously from our laboratory.[14,48] Here the reactions of Co_n^+ (n =2–20) with O_2 are presented from thermal energies to 10 eV in the center-of-mass frame. A variety of $Co_mO_2^+$, Co_mO^+, and Co_m^+ ($m \leqslant n$) product ions is observed, with the dioxide cluster ions dominating the products for all larger clusters. In this paper, we will refer to $Co_mO_2^+$ products as "cluster dioxides," Co_mO^+ products as "cluster monoxides," and Co_m^+ products as "cluster fragments." In all of these systems, there are two difficulties in obtaining reliable cross-section data, as discussed previously.[5–8] First, the cross sections have been corrected for overlap of adjacent mass peaks as long as the corrections are unambiguous. Second, the cross sections correspond to products formed only in single reactive collisions. Products formed in secondary reactions with O_2 are identified by examining the pressure dependence of the cross sections. On the basis of such studies, a complete set of figures for all Co_n^+ clusters (n=2–20) reacting with O_2 can be obtained from Ref. 49. Thermochemistry used to evaluate some of the threshold energies for the smallest clusters is listed in Table I.[23,48,50–54] Throughout the text, dissociation energies of the bare cluster cations are obtained from Ref. 23,53.

TABLE I. Bond energies and ionization energies from the literature (eV) (Uncertainties given in parentheses.)

	D_0	IE
Co	···	7.8810[a]
Co_2	⩽1.32[b]	⩽6.42[b]
Co_2^+	2.765 (0.001)[c]	···
CoO	3.94 (0.14)[d]	8.57 (0.15)[e]
	4.08 (0.09)[f]	8.71 (0.20)[e]
		9.0 (0.05)[g]
Co^+–O	3.25 (0.05)[h]	···
O_2	5.116 (0.002)[i]	12.071[i]
O	···	13.619[i]

[a]Reference 50.
[b]Reference 23.
[c]Reference 51.
[d]Reference 59.
[e]Calculated from $IE(CoO)=D_0(Co-O)+IE(Co)-D(Co^+-O)$.
[f]This work, see text.
[g]Reference 60.
[h]References 48, 52, and 53.
[i]Reference 54.

A. $Co_2^+ + O_2$

The kinetic-energy-dependent studies of the reaction of cobalt dimer with oxygen from thermal energies to 2 eV (CM) have previously been carried out in our laboratory.[14] Here we extend the kinetic-energy range examined to 10 eV. Only three products, Co_2O^+, CoO^+, and Co^+, are observed, as shown in Fig. 1, and exhibit energy dependences in good agreement with our previous results. In contrast, Guo *et al.* report two products at thermal energies (equivalent to the

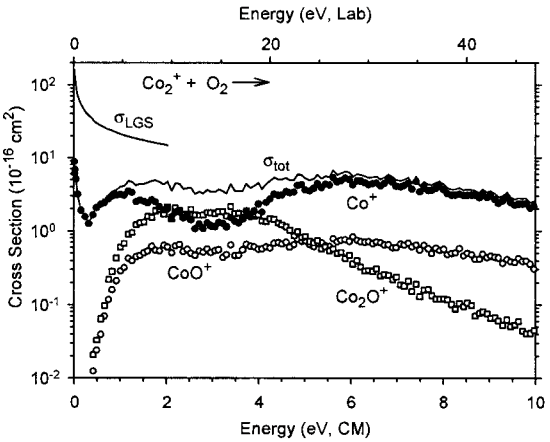

FIG. 1. Cross section for the reaction of Co_2^+ with O_2 as a function of collision energy in the center-of-mass (lower x axis) and laboratory (upper x axis) frames.

lowest-energy point shown in our results): Co^+ (70%) and $Co_2O_2^+$ (30%).[13] Presumably we do not observe the latter product because it is formed by collisional stabilization of the transiently formed $Co_2O_2^+$ complex in the high-pressure bath gas (He at 0.6 mTorr) in the flow tube studies. Under our single-collision conditions, the $Co_2O_2^+$ complex readily decomposes to Co^+ or back to reactants at thermal energies.

There are seven possible channels for this system, reactions (2)–(4). Reaction enthalpies at 0 K (with uncertainties in parentheses) are indicated for all reaction processes where thermochemical information is available, Table I.

$$Co_2^+ + O_2 \rightarrow Co_2O^+ + O, \tag{2}$$

$$\rightarrow CoO^+ + CoO, \quad 0.55(0.10), \tag{3a}$$

$$\rightarrow CoO^+ + Co + O, \quad 4.63(0.05), \tag{3b}$$

$$\rightarrow Co^+ + CoO_2, \quad < 0, \tag{4a}$$

$$\rightarrow Co^+ + Co + O_2, \quad 2.765(0.001), \tag{4b}$$

$$\rightarrow Co^+ + CoO + O, \quad 3.80(0.09), \tag{4c}$$

$$\rightarrow Co^+ + Co + 2O, \quad 7.881(0.002). \tag{4d}$$

Reaction (2) is the only channel that can form Co_2O^+, explaining why there is a single feature to the cross section over the entire energy range. The Co_2O^+ cross section rises rapidly from an energy near 0.4 eV, suggesting that reaction (2) is endothermic. It reaches a plateau above 2 eV and then declines above about 4 eV, corresponding with an increase in the Co^+ cross section. This behavior indicates that Co_2O^+ decomposes to $Co^+ + CoO$, which corresponds to the overall reaction (4c). Note that this pathway is favored over decomposing to $CoO^+ + Co$, process (3b), evident as the small increase in the CoO^+ cross section above the threshold energy for reaction (3b). The CoO^+ cross section begins near 0.4 eV, consistent with reaction (3a).

The dominant product over most of the energy range examined is the Co^+ fragment, which displays the most complicated energy dependence. The rise in the Co^+ cross section near 3.5 eV is coupled with the decrease in the Co_2O^+ cross section and can be attributed to reaction (4c), along with reaction (4b), simple CID. The CID cross section of Co_2^+ with Xe (Refs. 14 and 23) has a comparable magnitude to the Co^+ cross section observed here above 4 eV. Formation of Co^+ below 2.5 eV must be associated with reaction (4a), but the cross section exhibits both an exothermic feature as well as an endothermic feature beginning near 0.3 eV. Previous studies[14] investigated the dependence of this cross section on the internal energy of the Co_2^+ reactant and demonstrated that both features are observed across a broad range of internal energies, indicating that both probably result from reactions of ground state Co_2^+. Therefore, the two features can be attributed to different states of Co^+ or CoO_2 or different geometries of CoO_2, as discussed further below. Often the kinetic-energy dependence of exothermic ion-molecule reactions can be quantified by the Langevin-Gioumousis-Stevenson[55] (LGS) formula, $\sigma_{LGS} = \pi e (2\alpha/E)^{1/2}$ where α is the polarizability of O_2 (1.57 Å^3),[56] e is the charge on the electron, and E is the kinetic energy. In this system, the magnitude of the Co^+ cross section at thermal energies is much smaller than this prediction, $0.06 \pm 0.02 \sigma_{LGS}$, and declines more rapidly, $E^{-0.8 \pm 0.1}$. This kind of energy dependence can be a sign of a spin-forbidden reaction,[57] as discussed further below.

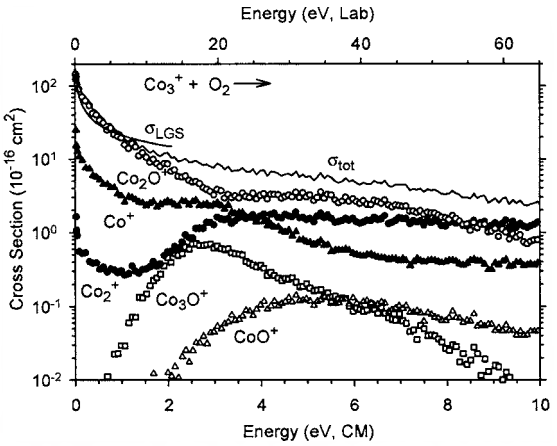

FIG. 2. Cross section for the reaction of Co_3^+ with O_2 as a function of collision energy in the center-of-mass (lower x axis) and laboratory (upper x axis) frames.

B. $Co_3^+ + O_2$

For the reaction of the cobalt trimer cation with O_2, five product ions are observed and some of them exhibit multiple features, Fig. 2. In agreement with these results, Guo *et al.* observe Co_2O^+ as the dominant product (60%) at thermal energies, with small amounts of Co^+ (10%) as well.[13] Guo *et al.* also observed $Co_2O_2^+$ (30%) in their work, whereas this product is not observed here. This suggests that this product may be the result of a secondary reaction, $Co_2O^+ + O_2 \rightarrow Co_2O_2^+ + O$.

In the cobalt trimer system, there are 20 possible pathways, reactions (5)–(9), for formation of product ions. Reaction enthalpies at 0 K are based on information from Table I and Ref. 23.

$$Co_3^+ + O_2 \rightarrow Co_3O^+ + O, \tag{5}$$

$$\rightarrow Co_2O^+ + CoO, \quad < 0, \tag{6a}$$

$$\rightarrow Co_2O^+ + Co + O, \tag{6b}$$

$$\rightarrow Co_2^+ + CoO_2, \quad < 0, \tag{7a}$$

$$\rightarrow Co_2^+ + Co + O_2, \quad 2.086(0.002), \tag{7b}$$

$$\rightarrow Co_2^+ + CoO + O, \quad 3.12(0.09), \tag{7c}$$

$$\rightarrow Co_2^+ + Co + 2O, \quad 7.20(0.01), \tag{7d}$$

$$\rightarrow CoO^+ + Co_2O, \tag{8a}$$

$$\rightarrow CoO^+ + CoO + Co, \quad 2.64(0.10), \tag{8b}$$

$$\rightarrow CoO^+ + Co_2 + O, \quad \geqslant 5.40(0.05), \tag{8c}$$

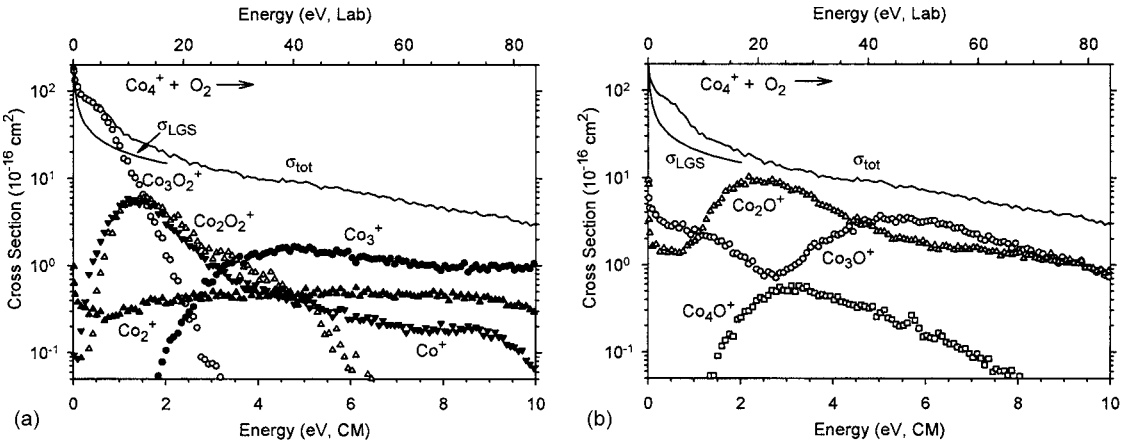

FIG. 3. Cross section for the reaction of Co_4^+ with O_2 as a function of collision energy in the center-of-mass (lower x axis) and laboratory (upper x axis) frames. Part (a) exhibits the cluster-dioxide and the cluster-fragment products. Part (b) shows the cluster-monoxide products.

$$\rightarrow CoO^+ + 2Co + O, \quad 6.72(0.05), \tag{8d}$$

$$\rightarrow Co^+ + Co_2O_2 \quad < 0, \tag{9a}$$

$$\rightarrow Co^+ + Co + CoO_2, \tag{9b}$$

$$\rightarrow Co^+ + 2CoO, \quad 1.81(0.13), \tag{9c}$$

$$\rightarrow Co^+ + Co_2 + O_2 \quad \geqslant 3.53(0.01), \tag{9d}$$

$$\rightarrow Co^+ + Co_2O + O, \tag{9e}$$

$$\rightarrow Co^+ + 2Co + O_2, \quad 4.85(0.01), \tag{9f}$$

$$\rightarrow Co^+ + Co + CoO + O, \quad 5.89(0.09), \tag{9g}$$

$$\rightarrow Co^+ + Co_2 + 2O, \quad \geqslant 8.65(0.01), \tag{9h}$$

$$\rightarrow Co^+ + 2Co + 2O, \quad 9.97(0.01). \tag{9i}$$

Among the cluster-monoxide products, Fig. 2, the dominant product at all energies is Co_2O^+. Reaction (6a) is the only pathway to which the exothermic portion of this cross section can be attributed. Within the experimental error, the total cross section for the reaction of cobalt trimer cation with oxygen equals σ_{LGS} at thermal energies, but declines more slowly than this prediction, $E^{-0.4\pm0.1}$, such that the experimental cross section is somewhat larger from 0.1 to 1.0 eV. For the Co_2O^+ cross section, a second feature beginning at about 3 eV must be the result of reaction (6b), which occurs by Co atom loss from Co_3O^+. The Co_3O^+ cross section reaches a maximum near 3 eV, verifying that this product decomposes to Co_2O^++Co. This primary product ion Co_3O^+ can be formed in only one path, the endothermic reaction (5). CoO^+ displays an endothermic cross section with an apparent threshold most consistent with reaction (8b), which corresponds to decomposition of the Co_2O^+ product formed in reaction (6a) into CoO^++Co. As in Fig. 1, this decomposition competes with the formation of Co^++CoO, reaction (9c). This latter pathway is thermodynamically favored, consistent with the larger cross section of Co^+ vs CoO^+ at high collision energies.

Metal cluster fragments are also observed as products, Fig. 2. The exothermic feature in the Co_2^+ cross section must be a result of reaction (7a) and the second feature starting near 1.5 eV corresponds primarily to reaction (7b), the simple CID process. Contributions from reaction (7c) are also possible and would correspond to a loss of CoO from a precursor Co_3O^+ product ion. This would be a minor dissociation channel for Co_3O^+ as it appears to dissociate primarily to Co_2O^++Co. The Co^+ product has a complicated energy dependence, including an exothermic feature that must be attributed to reaction (9a). On the basis of the discussion above, reaction (9c) surely contributes to the endothermic feature beginning near 1.5 eV. It is also likely that reaction (9f) contributes at higher energies, but CID with Xe exhibits Co_2^+ and Co^+ cross sections with relative magnitudes consistent with the present results only above about 7 eV.[23]

C. $Co_4^+ + O_2$

The $Co_4^+ + O_2$ system can generate 11 different product ions containing Co and there are at least 49 possible reaction pathways. At thermal energies, the dominance of the $Co_3O_2^+$ product ion agrees with the flow tube studies of Guo *et al.*, who observed only this product ion.[13] Figure 3 shows eight product ion cross sections observed in the reaction of Co_4^+ with O_2. As it is laborious to list all the reaction pathways, we shall do so only for the reactions observed.

$$Co_4^+ + O_2 \rightarrow Co_4O^+ + O, \tag{10}$$

$$\rightarrow Co_3O_2^+ + Co, \tag{11}$$

$$\rightarrow Co_3O^+ + CoO, \tag{12a}$$

$$\rightarrow Co_3O^+ + Co + O, \tag{12b}$$

$$\rightarrow Co_3^+ + Co + O_2 \quad 2.12(0.13), \tag{13a}$$

$$\rightarrow Co_3^+ + CoO + O, \quad 3.16(0.16), \tag{13b}$$

$$\rightarrow Co_2O_2^+ + Co_2, \quad < 0, \tag{14a}$$

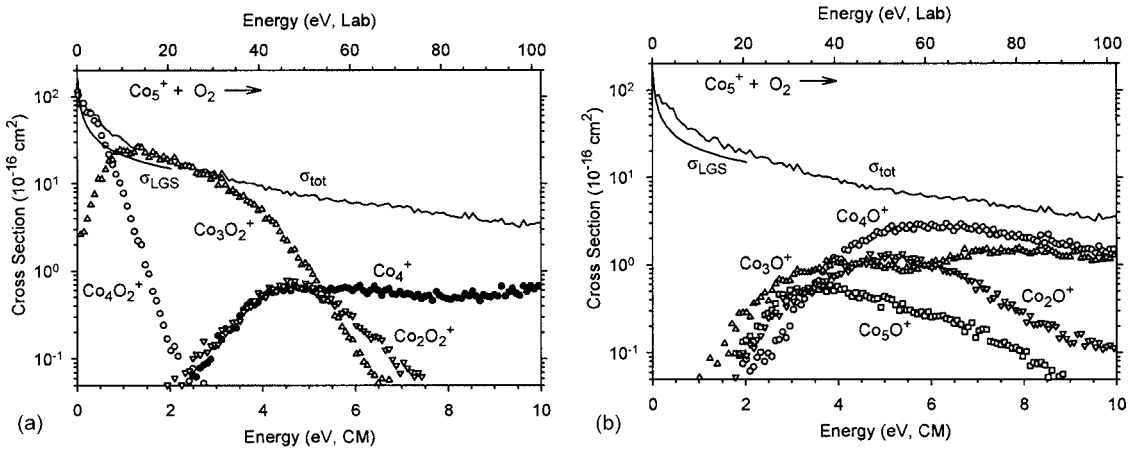

FIG. 4. Cross section for the reaction of Co_5^+ with O_2 as a function of collision energy in the center-of-mass (lower x axis) and laboratory (upper x axis) frames. Part (a) exhibits the cluster-dioxide and the cluster-fragment products. Part (b) shows the cluster-monoxide products.

$$\rightarrow Co_2O_2^+ + 2Co, \quad (14b)$$

$$\rightarrow Co_2O^+ + Co_2O, \quad < 0, \quad (15a)$$

$$\rightarrow Co_2O^+ + CoO + Co, \quad (15b)$$

$$\rightarrow Co_2O^+ + 2Co + O, \quad (15c)$$

$$\rightarrow Co_2^+ + Co_2O_2, \quad (16a)$$

$$\rightarrow Co_2^+ + 2CoO, \quad 1.16(0.13), \quad (16b)$$

$$\rightarrow Co_2^+ + CoO_2 + Co, \quad (16c)$$

$$\rightarrow Co_2^+ + 2Co + O_2, \quad 4.21(0.13), \quad (16d)$$

$$\rightarrow Co^+ + Co_2O_2 + Co, \quad (17a)$$

$$\rightarrow Co^+ + 2CoO + Co, \quad 3.93(0.18), \quad (17b)$$

$$\rightarrow Co^+ + 3Co + O_2, \quad 6.98(0.13). \quad (17c)$$

Many of these cross sections display complicated energy dependences. The cluster-dioxide product, $Co_3O_2^+$, can be formed in only a single pathway, reaction (11), accompanied by losing atomic Co. This cross section behaves as an exothermic reaction, declining with energy as $E^{-0.3\pm0.1}$ until 0.6 eV, somewhat more slowly than the predicted behavior of the LGS cross section. At our lowest energies, the magnitude measured here is slightly larger but within experimental error of this predicted collision cross section, by about 30%, a result discussed in more detail below. Above about 0.5 eV, the $Co_3O_2^+$ cross section decreases even faster with energy as the $Co_2O_2^+$ cross section rises. This indicates that $Co_3O_2^+$ dissociates by Co atom loss to form $Co_2O_2^+$, reaction (14b). On the basis of the results for the $Co_3^+ + O_2$ system, it is clear that $Co_3O_2^+$ dissociates preferentially by losing CoO to form Co_2O^+, reaction (15b), and also by Co^+ loss yielding Co_2O_2, reaction (17a). Both the Co_2O^+ and Co^+ product cross sections exhibit endothermic features that are consistent with such decompositions. The energy dependence for Co_3^+ formation is consistent with the simple CID process (13a). For Co_2^+, the exothermic cross section observed must be associated with reaction (16a), a minor decomposition route for Co_3O^+, whereas the endothermic portion of the cross section can be attributed to reaction (16b). It seems likely that Co_2^+ is formed at higher energies by the simple CID process, reaction (16c).

Figure 3(b) displays the monoxide products formed in this system. The primary Co_4O^+ product can only be formed along one endothermic pathway, reaction (10). The exothermic feature in the Co_3O^+ cross section must correspond to formation of a CoO neutral, reaction (12a), and the endothermic feature to Co+O formation, reaction (12b). This latter path is equivalent to dissociation of Co_4O^+ by Co atom loss. The correspondence of the peaks in the Co_4O^+ cross section and the onset of the endothermic feature in the Co_3O^+ confirm this. The Co_3O^+ product formed by both pathways can then dissociate by loss of a Co atom at still higher energies. This contributes to the low-energy endothermic feature in the Co_2O^+ cross section, reaction (15b), and at very high energies (above ~5 eV), reaction (15c). The cross section for Co_2O^+ also has an exothermic feature that must therefore correspond to the formation of $Co_2O^+ + Co_2O$, reaction (15a).

D. $Co_5^+ + O_2$

Figure 4 shows the product cross sections for reaction of Co_5^+ with O_2. At thermal energies, the dominance of the $Co_4O_2^+$ product ion agrees with the flow tube studies of Guo *et al.*, who observed only this product ion.[13] Eight of fourteen possible product ions containing Co are observed in our study. The cluster-dioxide products dominate the products at low energies and the monoxides dominate at higher energies. Of the cluster-dioxide products, the $Co_4O_2^+$ product can be formed in only a single pathway, accompanied by atomic Co. The $Co_4O_2^+ + Co$ channel is the dominant low-energy product and has a cross section with a magnitude comparable to σ_{LGS} at our lowest energies, but again declines more slowly, as $E^{-0.25\pm0.1}$ up to 0.5 eV. The cross section of $Co_4O_2^+$ behaves as an exothermic reaction and then declines more quickly with energy as the $Co_3O_2^+$ cross section rises. This clearly indicates that $Co_4O_2^+$ decomposes by Co atom loss. Above about 3 eV, the $Co_3O_2^+$ product cross section decreases more

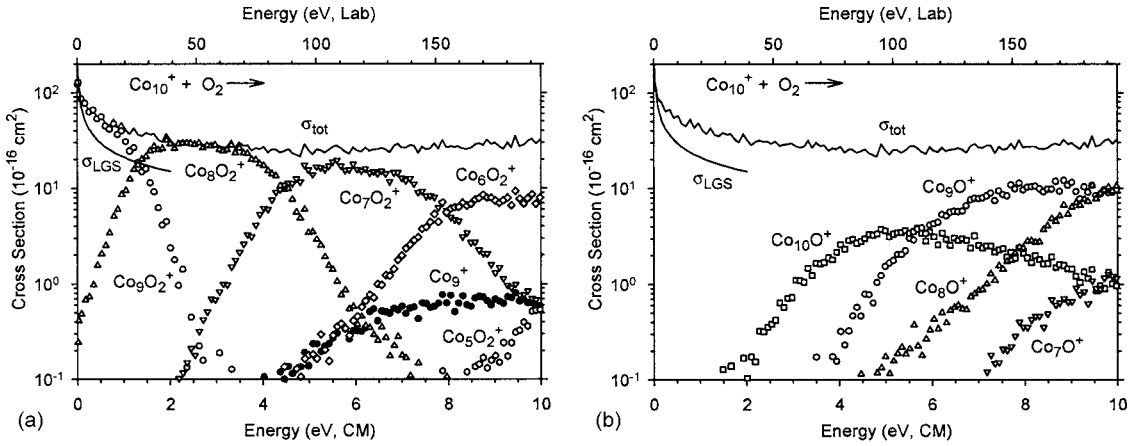

FIG. 5. Cross section for the reaction of Co_{10}^+ with O_2 as a function of collision energy in the center-of-mass (lower x axis) and laboratory (upper x axis) frames. Part (a) exhibits the cluster-dioxide and the cluster-fragment products. Part (b) shows the cluster-monoxide products.

rapidly with energy as the $Co_2O_2^+$ and Co_2O^+ cross sections rise. Simple CID to form Co_4^+ can begin at 2.84±0.16 eV (Ref. 23) and accounts for the major feature in the Co_4^+ cross section.

For the cluster-monoxide product ions, Fig. 4(b), Co_5O^+ is formed in an endothermic reaction along with an oxygen atom. Most of Co_4O^+ cross section must correspond to the formation of Co+O neutrals because the cross section rises as the Co_5O^+ falls. The Co_3O^+ cross section exhibits two distinct features that could result from reactions (18a)–(18c).

$$Co_5^+ + O_2 \rightarrow Co_3O^+ + Co_2O, \quad (18a)$$

$$\rightarrow Co_3O^+ + CoO + Co, \quad (18b)$$

$$\rightarrow Co_3O^+ + 2Co + O, \quad (18c)$$

$$\rightarrow Co_2O^+ + Co_2O + Co, \quad (19a)$$

$$\rightarrow Co_2O^+ + CoO + 2Co. \quad (19b)$$

The lowest-energy endothermic feature probably results from reaction (18b), because $Co_4O_2^+$ was shown to decompose to both $Co_3O_2^+$+Co and to Co_3O^++CoO in the reaction of the tetramer, Fig. 3. The second feature beginning near 5.5 eV corresponds to the dissociation of Co_4O^+ product by loss of Co, reaction (18c). The Co_2O^+ product potentially can be formed along three pathways: losing Co_2O neutral from a $Co_4O_2^+$ product, reaction (19a); losing CoO neutral from a $Co_3O_2^+$ precursor, reaction (19b); losing atomic Co from Co_3O^+ formed from reaction (18b), also corresponding to reaction (19b). At higher energies, contributing pathways cannot be determined unambiguously, as the number of neutral products possible increases and the thermochemistry for some of these is not known.

E. $Co_n^+ + O_2$ (n=6–20)

Although the number of possible reaction products and pathways increases rapidly with increasing reactant cluster size, the reactivity observed actually simplifies and there are strong similarities among the larger clusters. Figures 5 and 6 show the results for the reactions of Co_{10}^+ and Co_{16}^+ with dioxygen. These two systems are representative of the behavior of all clusters larger than Co_5^+. At thermal energies, the magnitudes of the total reaction cross sections match the σ_{LGS} prediction within the experimental error, except for Co_6^+ which is somewhat smaller, $(0.7\pm0.2)\times\sigma_{LGS}$. However, the reaction cross sections decline more slowly than σ_{LGS} for all

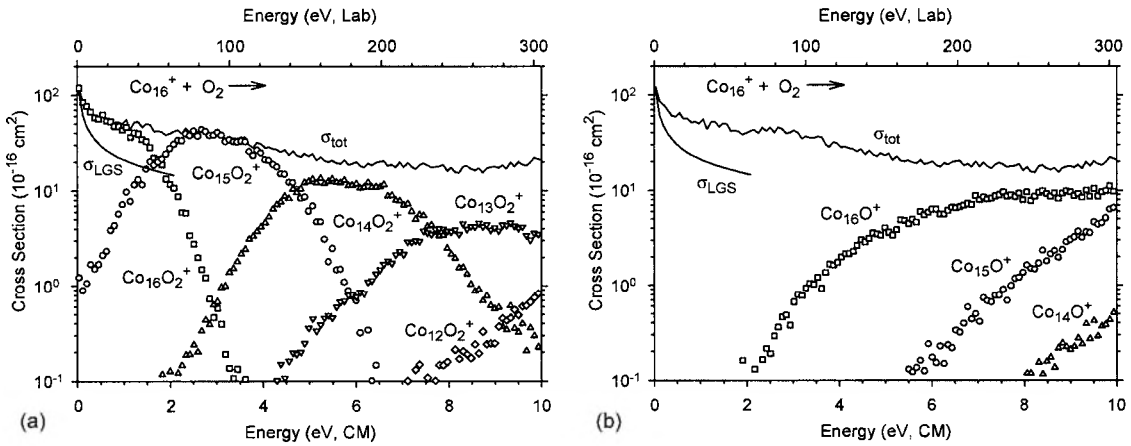

FIG. 6. Cross section for the reaction of Co_{16}^+ with O_2 as a function of collision energy in the center-of-mass (lower x axis) and laboratory (upper x axis) frames. Part (a) exhibits the cluster-dioxide and the cluster-fragment products. Part (b) shows the cluster-monoxide products.

cluster sizes, averaging $E^{-0.27\pm0.05}$ for $n=6-20$, for kinetic energies ranging from thermal up to about 0.5 eV. Thus the cross-section magnitudes exceed σ_{LGS} at these lower energies, except for Co_6^+, as discussed further below.

Cluster-dioxide ions are the dominant products at low energies, Figs. 5(a) and 6(a), in agreement with the flow tube studies of Guo *et al.*[13] As the cluster reactants increase in size, the energy range over which this is true increases from below about 6 eV for Co_6^+ to about 9 eV for Co_{20}^+. It is clear that the cluster dioxides formed at low energies dissociate by sequential loss of cobalt atoms as the energy is increased. This is evident from the observation that the cross sections for $Co_mO_2^+$ products decline as the $Co_{m-1}O_2^+$ cross sections rise. If there are any features that might correspond to the formation of molecular Co_{n-m} neutrals, they are negligible within our experimental signal-to-noise ratio. Although the product distributions are similar for larger clusters, different sized clusters are distinguished by the largest $Co_mO_2^+$ product (highest m value) observed. This is $Co_{n-1}O_2^+$ for Co_4^+ to Co_{10}^+. The $Co_nO_2^+$ adduct is not observed until Co_{11}^+ and gradually increases in importance until it dominates at low energies for Co_{15}^+ and larger clusters. These observations are not dependent on the pressure of the O_2 reactant, so that collision stabilization is not responsible for the $Co_nO_2^+$ products. As discussed below, these changes in the dominant $Co_mO_2^+$ product observed can be attributed primarily to increasing lifetimes as the clusters get larger.

For $n=6-20$, the cluster-oxide products Co_nO^+ exhibit thresholds in the vicinity of 1.4–2.1 eV. The formation of these products suffers from competition with the favored cluster-dioxide products as discussed below. As the energy is increased, these products dissociate by sequentially losing cobalt atoms, Figs. 5(b) and 6(b). We observe that the $Co_{n-2}O^+$ cross sections show two obvious features for $n \leq 12$, as shown, for example, in Fig. 5(b), in which the second feature begins somewhere near 7 eV. The higher-energy feature is clearly a result of concomitant formation of 2Co +O, formed by Co loss from the $Co_{n-1}O^+$ product, whereas the lower-energy feature can be attributed to the formation of CoO+Co neutral products. These pathways are analogous to reactions (18b) and (18c) for reactions of the Co_5^+ cluster. For these larger reactant cluster ions ($n=6-20$), the cluster-fragment ions are minor products. Only the Co_{n-1}^+ for $n=6-12$ ionic products were observed below 10 eV. Other fragments were either not observed or their overall intensity was much less than 1% of all products. Certainly small amounts of such fragments are probably formed but these pathways are not quantitatively important for larger Co_n^+ clusters.

IV. DISCUSSION

A. Reaction mechanism

The mechanism for the reactions of cobalt cluster ions with O_2 appears fairly straightforward. Dissociative chemisorption of the O_2 molecule on the cluster surface heats the cluster strongly (by 3.5–5.5 eV on the basis of the thermochemistry derived below) and dissociation ensues. Cobalt-oxygen bonds are stronger than cobalt-cobalt bonds, such that dissociation is dominated by cobalt atom loss to form cluster-dioxide ions. Formation of primary cluster-monoxide products, Co_nO^+, occurs by loss of an oxygen atom, which is less efficient. Competition between these two channels must occur early in the reaction scheme, because cobalt and oxygen atom loss has to occur from the transient $Co_nO_2^+$ intermediate. This seems reasonable as dissociation cools the remaining cluster such that subsequent dissociations must occur primarily along the lowest-energy pathways available, typically Co atom loss. In addition to atomic loss processes, loss of molecular products such as CoO and Co_2O from the transient $Co_nO_2^+$ can also occur, especially from smaller clusters. Elimination of CoO from the $Co_nO_2^+$ precursor can be readily identified from the exothermic formation of the $Co_{n-1}O^+$ product for $n=3$ and 4, and CoO loss from the $Co_{n-1}O_2^+$ product persists to larger cluster sizes ($n=5-12$). Apparently, loss of CoO from the initially formed $Co_nO_2^+$ adduct does not compete with Co loss over this range of cluster sizes. As the kinetic energy of the reactants is increased, the primary products dissociate further with loss of atomic cobalt being the most prominent dissociation process for both cluster dioxides and monoxides. Cluster fragments, Co_{n-x}^+, are observed as minor products. Their cross sections have relatively low magnitudes, less than 1 Å^2, and primarily result from simple CID processes for $n=6-12$.

For barrierless, exothermic ion-molecule reactions, the LGS expression[55] can often be used to predict the reaction cross section. Because σ_{LGS} is determined by the polarizability of the neutral gas, it is the same for all cluster ion sizes. Examination of Figs. 1–6 shows that at the very lowest energies, the total reaction cross sections have similar magnitudes and follow an energy dependence that declines more slowly than the $E^{-1/2}$ LGS prediction. Within the experimental uncertainties, the cross sections at our lowest energies for all clusters but $n=2$ and 6 agree with the collision cross section calculated according to the LGS model, indicating that the reactions occur with unit efficiency at thermal energies. As the collision energy is increased, however, the total cross sections for the reactions of Co_n^+ ($n=3-20$) with O_2 exceed σ_{LGS} at slightly elevated energies (up to 0.5–1 eV). This phenomenon has also been observed in the reactions of iron, chromium, vanadium, and nickel cluster ions with O_2 as reported previously in our laboratory,[5–8] and by Jarrold and Bower in their study of the reactions of aluminum cluster cations with O_2.[58] They reasoned that the predictions of the LGS model failed because the physical size of the cluster exceeds σ_{LGS} at even modest kinetic energies.

B. Cluster-dioxide bond energies, Co_n^+–2O

The bond energies, $D(Co_n^+-2O)$, can be directly obtained by using Eq. (1) to analyze cross sections for cluster dioxides formed in endothermic processes. For smaller clusters, $n=4-16$, the cross sections for the $Co_{n-2}O_2^+$ product were analyzed. [It can be noted that the kinetic shifts in these cases range from negligible for $n \leq 6$ to substantial, ~3 eV, for $n=20$, making it unambiguous that the kinetic analysis included in Eq. (1) is required to yield reasonable thermochemistry.] For clusters larger than $n=15$, cross sections for

TABLE II. Summary of parameters used in Eq. (1) for analysis of $Co_mO_2^+$ cross sections and relative energy measurements for the dissociation $Co_mO_2^+ \rightarrow Co_{m-1}O_2^+ + Co$. (Uncertainties in parentheses.)

m	Reactant cluster size, n	σ_0	N	E_0 (eV)	ΔE (eV)[a]
2	4	12.1(0.6)	1.8(0.2)	0.67(0.06)	···
3	5	32.3(2.4)	1.9(0.2)	0.37(0.06)	3.20(0.23)
4	6	30.6(2.2)	1.8(0.2)	1.04(0.05)	2.78(0.19)
5	7	25.8(4.6)	1.8(0.2)	1.05(0.05)	2.94(0.22)
6	8	43.6(7.4)	1.8(0.2)	1.01(0.05)	3.02(0.16)
7	9	41.9(3.8)	1.8(0.1)	0.91(0.03)	2.94(0.22)
8	10	31.1(4.0)	1.8(0.2)	0.83(0.04)	2.93(0.16)
9	11	26.4(5.1)	1.8(0.2)	1.20(0.06)	2.59(0.17)
10	12	21.6(4.0)	1.7(0.2)	1.31(0.07)	3.18(0.20)
11	13	23.0(4.4)	1.5(0.1)	1.58(0.08)	3.37(0.26)
12	14	15.5(3.6)	1.8(0.2)	1.62(0.09)	3.14(0.21)
13	15	43.6(4.6)	1.5(0.2)	2.01(0.10)	3.41(0.18)
14	16	20.8(4.6)	1.9(0.2)	2.20(0.10)	3.42(0.27)
15	16	16.3(4.2)	2.2(0.2)	0.62(0.14)	3.20(0.20)
	17	26.6(3.4)	1.9(0.2)	2.39(0.11)	3.16(0.26)
16	17	19.1(4.8)	2.3(0.2)	0.99(0.10)	3.13(0.22)
	18	12.4(1.9)	2.0(0.2)	2.48(0.12)	3.49(0.29)
17	18	25.8(5.6)	1.9(0.2)	1.30(0.07)	3.09(0.22)
	19	19.1(4.1)	1.9(0.3)	2.68(0.15)	3.36(0.28)
18	19	32.1(2.4)	1.7(0.2)	1.54(0.08)	3.27(0.20)
	20	8.4(1.4)	2.1(0.2)	2.58(0.13)	3.43(0.30)
19	20	19.8(1.9)	1.9(0.2)	1.56(0.10)	3.02(0.25)

[a]Weighted average of two methods discussed in the text.

the $Co_{n-1}O_2^+$ product were also analyzed. The optimized parameters used in Eq. (1) to reproduce the data are listed in Table II and converted to $Co_{n-x}O_2^+$ (x=1,2) thermochemistry by using Eq. (20), where $D(Co_{n-x}^+ - xCo)$ values are taken from Ref. 23.

$$D(Co_{n-x}^+ - 2O) = D(Co_{n-x}^+ - xCo) + D(O_2) - E_0. \quad (20)$$

The bond energies derived from these direct threshold determinations are listed in Table III to allow comparison between values from different systems and with the upper and lower limits derived below. Bond energies obtained from analyses of $Co_{n-2}O_2^+$ cross sections exceed those extracted from $Co_{n-1}O_2^+$ cross sections by an average of 2.30±0.35 eV. In general, bond energies derived from thresholds can be too low for a number of reasons including barriers to the process, competition with other more favorable channels, or kinetic shifts. The only means whereby a threshold can be lower than the true threshold (thus giving a bond energy that is too high) is if there are unaccounted sources of energy available, which seems unlikely in these systems. Therefore, the larger bond energies are more likely to be correct, as verified below.

Another way of obtaining information regarding the cluster dioxides is to examine the energy dependence of the $Co_{n-x}O_2^+$ clusters formed by sequential loss of Co atoms. The relative thresholds for these reactions can be measured fairly routinely, thereby bypassing questions regarding internal energies of the reactant clusters. Kinetic shifts should also cancel to a large extent although there is the possibility that these differences may represent upper limits to the true thermodynamic differences because of different kinetic shifts for subsequent reactions. Such an interpretation represents a "model-free" analysis of the energetics as originally outlined elsewhere.[5] This analysis was accomplished in two simple ways and relies on the shapes of the $Co_{n-x}O_2^+$ cross sections being similar in their threshold regions. First, the average energy difference between the cross sections for sequential cluster-dioxide products, i.e., $Co_{n-x}O_2^+$ and $Co_{n-x-1}O_2^+$, was measured from semilogarithmic plots of the data like that shown in Figs. 4–6 and Ref. 49. Second, the cross-section data on linear plots were linearly extrapolated to zero cross section and the difference between the intercepts on the energy axis for sequential cluster-dioxide products was taken as the energy difference. In both cases, these energy differences ΔE correspond to bond energies for $Co_{n-x-1}O_2^+ - Co$ and their averages are listed in Table II. To compare these values to the $Co_mO_2^+$ thermochemistry obtained above, we convert to $D(Co_m^+ - 2O)$ using Eq. (21), where $m=n-x$.

$$D(Co_m^+ - 2O) = D(Co_{m-1}O_2^+ - Co) + D(Co_{m-1}^+ - 2O) - D(Co_{m-1}^+ - Co). \quad (21)$$

This equation relies on the $Co_{m-1}^+ - 2O$ bond energies for the next smallest cluster, hence, the values listed in Table III derived from these relative threshold measurements are calculated using the average value for the next smallest cluster. This average is calculated from all available values (those directly measured and the relative values).

It can be seen from Table III and Fig. 7 that the agreement between the direct and relative measurements from loss of two atoms is fairly good, certainly within the experimental error of either determination. The average values listed in

TABLE III. Summary of Co_m^+–2O bond energies (in eV) from several sources. (Uncertainties in parentheses.)

m	Lower limit[a]	Upper limit[b]	Direct measurement[c]	Relative measurement[d]	Average[e]
2		9.33(0.13)	8.65(0.15)	···	8.65(0.15)
3	7.24(0.13)	10.08(0.21)	9.70(0.21)	9.76(0.27)	9.72(0.17)
4	7.96(0.16)	11.27(0.24)	10.22(0.25)	10.38(0.29)	10.29(0.19)
5	8.43(0.18)	11.36(0.25)	10.30(0.25)	10.39(0.33)	10.33(0.20)
6	8.06(0.17)	11.19(0.27)	10.17(0.27)	10.04(0.31)	10.11(0.20)
7	8.26(0.21)	11.19(0.26)	10.27(0.26)	10.12(0.34)	10.21(0.21)
8	8.05(0.15)	11.00(0.21)	10.16(0.21)	10.00(0.34)	10.12(0.18)
9	8.07(0.14)	11.32(0.29)	10.11(0.29)	9.78(0.29)	9.95(0.21)
10	8.37(0.25)	11.78(0.38)	10.46(0.38)	10.18(0.32)	10.30(0.25)
11	8.53(0.28)	12.17(0.41)	10.58(0.42)	10.42(0.44)	10.51(0.30)
12	8.76(0.30)	11.90(0.46)	10.27(0.47)	10.24(0.46)	10.25(0.33)
13	8.26(0.35)	12.20(0.52)	10.18(0.53)	10.02(0.48)	10.09(0.36)
14	9.06(0.38)	12.74(0.54)	10.55(0.55)	10.37(0.57)	10.46(0.40)
15	5.116(0.002)[f]	8.80(0.38)[a]	8.17(0.40)	9.72(0.57)	
	8.80(0.38)	12.39(0.57)	9.99(0.58)	9.68(0.61)	9.84(0.42)
16	5.116(0.002)[f]	8.71(0.43)[a]	7.71(0.44)	9.29(0.61)	
	8.71(0.43)	12.56(0.71)	10.07(0.72)	9.65(0.64)	9.84(0.48)
17	5.116(0.002)[f]	8.97(0.56)[a]	7.66(0.56)	9.34(0.68)	
	8.97(0.56)	12.68(0.72)	9.99(0.74)	9.61(0.70)	9.79(0.51)
18	5.116(0.002)[f]	8.83(0.46)[a]	7.28(0.47)	9.21(0.78)	
	8.83(0.46)	12.54(0.65)	9.95(0.66)	9.37(0.81)	9.72(0.51)
19	5.116(0.002)[f]	8.83(0.46)[a]	7.26(0.47)	9.03(0.73)	

[a]Sum of bond energies for loss of one Co atom plus $D(O_2)$, except as noted.
[b]Sum of bond energies for loss of two Co atoms plus $D(O_2)$, except as noted.
[c]Calculated from direct threshold measurements listed in Table II using Eq. (20).
[d]Calculated from relative threshold measurements listed in Table II using Eq. (21).
[e]Weighted average of the direct and relative measurements. Best values.
[f]$D(O_2)$.

Table III are therefore believed to be our best thermochemical information for the cluster dioxides. For $D(Co_m^+–2O)$ bond energies, $m \geq 15$, the agreement between the direct and relative values is quite good for the bond energies determined from loss of two atoms, with an mean absolute deviation of 0.42±0.11 eV. For bond energies determined from loss of only a single atom, the values are considerably lower and agreement between the direct and relative values is worse, with a mean absolute deviation of 1.70±0.15 eV. The fact that the former values yield a consistent trend in the Co_m^+–2O bond energies as a function of cluster size confirms that the latter values are less accurate than the former.

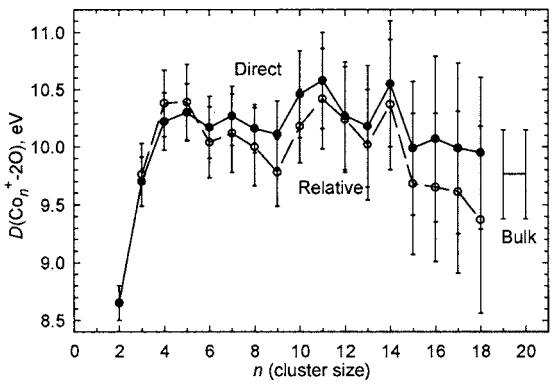

FIG. 7. Comparison of the dioxide bond energies obtained from relative (open circles) and direct (solid circles) measurements listed in Table III. The bulk-phase range is calculated from the average of experimental adsorption enthalpies of O_2 on several polycrystalline Co surfaces (Refs. 62–64).

After analyzing the endothermic reaction cross sections, it is worth considering the qualitative characteristics of the cluster-dioxide cross sections to assess the accuracy of the cluster-dioxide bond energies. First, we observe that the formation of the $Co_{n-2}O_2^+$ cluster is clearly endothermic (or thermoneutral) for all reactant cluster ions studied. Therefore, an upper limit to the binding energy of two oxygen atoms to the Co_{n-2}^+ cluster, $D(Co_{n-2}^+–2O)$, equals $D(Co_{n-2}^+–Co)+D(Co_{n-1}^+–Co)+D(O_2)$. Upper limits derived in this manner are listed in Table III. For $n \geq 15$, the formation of $Co_{n-1}O_2^+$ also appears to be endothermic, which would suggest that $D(Co_{n-1}^+–2O) \leq D(Co_{n-1}^+–Co)+D(O_2)$, values also listed in Table III. It is possible that the appearance of these cross sections is controlled not by the thermodynamics but by the lifetimes of these products. This possibility considers that loss of Co atoms from $Co_nO_2^+$, $n \geq 15$, is still an exothermic process (thermoneutral for $n=14$), but the average time required for this dissociation is longer than the 10^{-4} s available experimentally. Second, lower limits to the Co_n^+–2O bond energies can be obtained from observations of exothermic reactions. Cobalt clusters from $n=4–14$ clearly react exothermically with oxygen to form $Co_{n-1}O_2^+$+Co. This is the most probable reaction product at low energies, accounting for nearly 100% of the total cross section at thermal energies. The lower limits obtained for $D(Co_{n-1}^+–2O) \geq D(Co_{n-1}^+–Co)+D(O_2)$ are also listed in Table III. For larger clusters, for $n \geq 15$, the formation of $Co_nO_2^+$ is clearly exothermic, indicating that $D(Co_n^+–2O) \geq D(O_2)$.

TABLE IV. Summary of parameters used in Eq. (1) for the analysis of $Co_n^+ + O_2 \rightarrow Co_nO^+ + O$ cross sections and calculated bond energies. (Uncertainties in parentheses.)

n	σ_0	N	E_0 (eV)	$D(Co_n^+-O)$ (eV)[a]
2	2.9(0.3)	1.5(0.2)	0.65(0.06)	4.46(0.06)
3	0.5(0.1)	2.4(0.2)	0.84(0.08)	4.27(0.08)
4	0.7(0.1)	1.8(0.2)	1.10(0.09)	4.01(0.09)
5	0.6(0.2)	1.7(0.2)	1.53(0.10)	3.58(0.10)
6	0.8(0.2)	1.8(0.2)	1.93(0.12)	3.18(0.12)
7	1.2(0.3)	1.8(0.2)	1.95(0.12)	3.16(0.12)
8	2.4(0.6)	1.5(0.2)	2.09(0.10)	3.02(0.10)
9	2.1(0.5)	1.7(0.2)	1.64(0.09)	3.47(0.09)
10	2.9(0.6)	1.6(0.1)	1.68(0.08)	3.43(0.08)
11	3.5(0.7)	1.5(0.1)	1.70(0.09)	3.41(0.09)
12	4.0(1.0)	1.5(0.1)	1.76(0.09)	3.35(0.09)
13	2.2(0.7)	2.0(0.2)	1.47(0.10)	3.64(0.10)
14	2.9(1.0)	1.9(0.2)	1.55(0.10)	3.56(0.10)
15	2.4(0.4)	2.0(0.2)	1.40(0.11)	3.71(0.11)
16	2.4(0.3)	2.0(0.2)	1.71(0.14)	3.40(0.14)
17	3.2(0.6)	1.9(0.2)	1.82(0.16)	3.29(0.16)
18	1.9(0.3)	2.2(0.2)	1.69(0.16)	3.42(0.16)
19	1.8(0.8)	2.3(0.2)	1.68(0.17)	3.43(0.17)
20	1.8(0.3)	2.3(0.2)	1.74(0.16)	3.37(0.16)

[a]Values are lower limits to the true bond energies except for n=2 and 3. See text.

From Table III, we can see that the average values from direct and relative measurements for $n \leqslant 14$ agree with the lower and upper limits calculated by loss of one and two cobalt atoms being exothermic and endothermic, respectively, helping to confirm the accuracy of these results. For $n \geqslant 15$, the average values also fall in the range determined by loss of one and two cobalt atoms being exothermic and endothermic, respectively. Thus, the appearances of the $Co_{n-1}O_2^+$ cross sections for larger clusters are not good indicators of the endothermicity or exothermicity of the particular process and are influenced by lifetime effects. This conclusion is similar to the reactions of nickel cluster cations with oxygen,[8] but contrast with the results for iron, vanadium, and chromium cluster ion reactivity with O_2.[5–7]

C. Cluster-monoxide bond energies, Co_n^+–O

As a first approximation to the cluster-monoxide bond energies, we can assume that the two oxygen bonds in the $Co_nO_2^+$ species are similar, i.e., that $D(Co_n^+-O)$ is approximately half the $D(Co_n^+-2O)$ values listed in Table III. This estimate gives Co_n^+–O bond dissociation energies smaller than $D(O_2)$ for n=2,3,15–18 and comparable to $D(O_2)$ for n=4–14. This indicates that formation of Co_nO^+ in reaction (22) should be endothermic or thermoneutral, in agreement with our experimental observations (Figs. 1–6 and Ref. 49).

$$Co_n^+ + O_2 \rightarrow Co_nO^+ + O. \quad (22)$$

Reaction (22) is analyzed using Eq. (1) with optimized parameters listed in Table IV. (It can be noted that the kinetic shifts in these cases range from small, ~0.3 eV, for n=6 to substantial, ~1.7 eV, for n=20, making it unambiguous that the kinetic analysis included in Eq. (1) is required to yield reasonable thermochemistry.) The threshold energies are converted to bond energies using $D(Co_n^+-O)=D(O_2)-E_0(22)$, where $E_0(22)$ is the threshold measured for reaction (22), and the resulting values are also given in Table IV. Figure 8 shows that these values fall well below $D(Co_n^+-2O)/2$ for all clusters but n=2 and 3. The Co_nO^+ species are minor products for most cluster sizes and are in direct competition with formation of the cluster dioxides. The competition between losing an oxygen atom from the $Co_nO_2^+$ transient intermediate to form the cluster monoxides Co_nO^+ in reaction (22) and losing a cobalt atom to form $Co_{n-1}O_2^+$, a much more favorable process energetically, probably accounts for the high apparent thresholds observed for the Co_nO^+ products. It is also possible that that there are barriers along the potential-energy surface for the O atom loss pathway. In any case, it is clear that the thresholds observed for the $Co_nO^+ + O$ reaction channel are not reliable measurements of Co_nO^+ thermochemistry and provide only lower limits of $D(Co_n^+-O)$, except possibly for n=2 and 3.

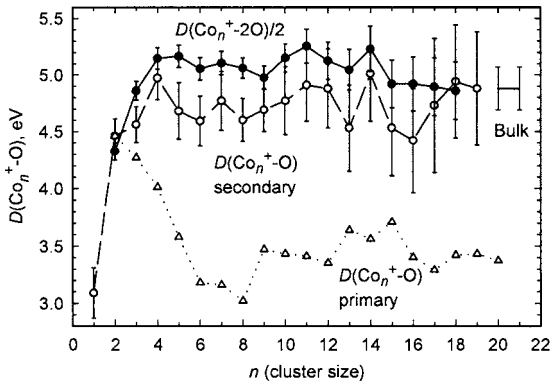

FIG. 8. Comparison of half the cluster-dioxide bond energies (solid circles, average values from Table III) with monoxide bond energies obtained from the primary reactions (open triangles, Table IV) and the secondary reactions (open circles, Table V). The bulk-phase range is calculated from the average of the experimental adsorption enthalpies of O_2 on several polycrystalline Co surfaces (Refs. 62–64).

The thresholds for reaction (23) provide an alternative method of deriving Co_n^+–O bond energies,

$$Co_n^+ + O_2 \rightarrow Co_{n-1}O^+ + Co + O. \quad (23)$$

Specifically, these threshold energies can be converted to bond energies using $D(Co_{n-1}^+-O)=D(O_2)+D(Co_{n-1}^+-Co)-E_0(23)$, where $E_0(23)$ is the threshold measured for reaction (23) and the bond energies of the bare cobalt cluster ions have been measured previously.[23] The optimized parameters using an analysis of the cross sections with Eq. (1) are listed in Table V, along with the bond dissociation energies of Co_n^+–O obtained from these thresholds using the equation noted above. In the case of $D(Co_2^+-O)$, the values obtained from the primary and secondary reactions, processes (22) and (23), are in good agreement. For larger clusters, a comparison of the values from Tables IV and V (Fig. 8) makes it evident that the primary monoxide bond energies are systematically lower than the secondary monoxide bond energies, by an average of 1.30±0.26 eV for $n \geqslant 4$. Although this discrepancy could be a result of barriers to the primary reaction, such barriers would have to occur in the exit channel as the initial reaction with O_2 is clearly unactivated on the basis of

TABLE V. Summary of parameters used in Eq. (1) for the analysis of $Co_{n+1}^+ + O_2 \rightarrow Co_nO^+ + Co + O$ cross sections and calculated bond energies. (Uncertainties in parentheses.)

n	σ_0	N	E_0 (eV)	$D(Co_n^+-O)$ (eV)
1	1.0(0.1)	2.2(0.4)	0.55(0.07)[a]	3.25(0.05)[b]
2	3.2(1.0)	1.4(0.2)	2.74(0.15)	4.46(0.15)
3	4.5(1.0)	1.6(0.2)	2.67(0.10)	4.56(0.16)
4	4.7(1.0)	1.4(0.2)	2.98(0.11)	4.97(0.19)
5	3.0(1.0)	1.6(0.2)	3.74(0.17)	4.68(0.25)
6	5.7(1.6)	1.7(0.2)	3.45(0.14)	4.59(0.22)
7	9.0(2.8)	1.6(0.2)	3.48(0.16)	4.77(0.26)
8	7.7(1.1)	1.6(0.1)	3.44(0.12)	4.60(0.19)
9	9.3(2.2)	1.6(0.2)	3.37(0.13)	4.69(0.19)
10	8.3(2.2)	1.5(0.2)	3.59(0.17)	4.77(0.30)
11	7.5(1.5)	1.6(0.1)	3.61(0.15)	4.91(0.32)
12	12.2(2.7)	1.4(0.2)	3.87(0.17)	4.88(0.35)
13	6.6(1.6)	1.7(0.1)	3.72(0.16)	4.53(0.38)
14	4.6(0.5)	1.7(0.2)	4.03(0.19)	5.01(0.42)
15	4.6(0.7)	2.0(0.2)	4.26(0.18)	4.53(0.42)
16	6.0(0.9)	2.0(0.2)	4.28(0.17)	4.42(0.46)
17	4.2(0.7)	2.0(0.2)	4.23(0.19)	4.73(0.59)
18	3.5(1.2)	1.7(0.3)	3.88(0.19)	4.94(0.50)
19	3.0(1.0)	1.6(0.3)	3.94(0.19)	4.88(0.50)

[a]Threshold for $CoO^+ + CoO$ formation.
[b]References 48, 52, and 53.

the results for the dioxide products. As loss of a single oxygen atom from the $Co_nO_2^+$ intermediates is unlikely to have a reverse activation barrier, it seems more likely that the low primary monoxide bond energies are the result of thresholds elevated by competition with the much more likely dioxide channels. The secondary reaction (23) does not exhibit direct effects of this competition because their precursor, Co_nO^+, cannot form cluster dioxides and prefers to decompose by Co atom loss.

D. Neutral cobalt cluster-oxide bond energies

In the dimer reaction, $Co_2^+ + O_2 \rightarrow CoO^+ + CoO$, the threshold obtained (Table V) can be used to yield the bond energy of the neutral CoO molecule given the $D(Co^+-O)$, $D(Co^+-Co)$, and $D(O-O)$ bond energies in Table I. We obtain $D(Co-O)=4.08\pm0.09$ eV, which agrees well with an evaluated value from Knudsen cell measurements, 3.94 ± 0.14 eV,[59] and with a preliminary value obtained from this same reaction, 4.24 ± 0.21 eV.[48,52,53] By combining the bond energies of the ion and neutral cobalt oxide with the ionization energy (IE) of cobalt atom (Table I), we can also derive an improved ionization energy for CoO of 8.71 ± 0.10 eV. This agrees within the experimental error with the only directly measured IE value of 9.0 ± 0.5 eV.[60]

Confirmation of this thermochemistry comes from reactions of larger clusters. For example, reaction of Co_4^+ with O_2 yields Co_3O^+ in an exothermic reaction that must correspond to formation of a CoO neutral, reaction (12a). Given $D(Co_3^+-O)$ in Table V, this indicates that $D(Co-O) > 2.68\pm0.21$ eV, consistent with the thermochemistry above. For the reactions, $Co_n^+ + O_2 \rightarrow Co_{n-2}O^+ + (2Co+O)$ for $n=4$ and 5, we modeled the lowest-energy endothermic feature of the $Co_{n-2}O^+$ cross sections (after subtracting a model of the exothermic reactivity for $n=4$) and obtained thresholds of 0.93 ± 0.12 ($n=4$) and 1.67 ± 0.11 ($n=5$) eV. Given the bond energies of $D(Co_2^+-O)$ and $D(Co_3^+-O)$ obtained above (Table V), the total binding energy of the $(2Co+O)$ neutral products is found to be 3.93 ± 0.23 and 3.85 ± 0.29 eV, respectively. These values are in good agreement with the $D(Co-O)$ values obtained here and from Ref. 59, indicating that the neutral products correspond to CoO+Co, reactions (15b) and (18b). Comparable conclusions are drawn for the analogous reactions for other clusters.

In the tetramer system, formation of Co_2O^+ exhibits an exothermic cross-section feature that must be attributed to reaction (15a). This indicates that the atomization energy of the Co_2O neutral product must exceed 4.82 ± 0.24 eV. In the pentamer system, the lowest-energy endothermic feature of the Co_2O^+ cross section is analyzed to give a threshold of 1.77 ± 0.18 eV. The total binding energy of the $(3Co+O)$ products is 5.93 ± 0.31 eV, which means this channel cannot be CoO+2Co, but is consistent with the lower limit just established for Co_2O. This means that the lowest-energy endothermic feature of Co_2O^+ can be attributed to reaction (19a), forming Co_2O+Co. Given $D(Co_2) \leq 1.32$ eV and $D(Co-O)=4.08\pm0.09$ eV (Table I), this means that $D(Co_2-O) \geq 4.61\pm0.31$ eV and $D(OCo-Co) = 1.85\pm0.32$ eV.

The cobalt dimer and trimer cluster cations react with oxygen to form $Co_{n-1}^+ + CoO_2$ in exothermic pathways, reactions (4a) and (7a). This means that the atomization energy of CoO_2 exceeds 7.881 ± 0.002 and 7.16 ± 0.13 eV, respectively, or equivalently that dissociation of CoO_2 to $Co+O_2$ requires more than 2.765 ± 0.001 and 2.04 ± 0.13 eV, respectively. As mentioned above, in the reaction of the dimer cation, the Co^+ cross section exhibits both an exothermic feature as well as an endothermic feature below 2.5 eV, which must both be attributed to reaction (4a). We analyzed the endothermic feature after subtracting a model of the exothermic reactivity in these systems (using a simple power law) and obtained a threshold of 0.41 ± 0.11 eV. This endothermic feature must correspond to formation of an excited state of Co^+ or CoO_2, perhaps along a surface having a different spin. Several theoretical calculations have been performed on the CoO_2 molecule, obtaining $Co-O_2$ bond energies for the ground-state dioxo species of 2.13,[21] 3.4,[20] and 4.03 eV.[19] Only the latter two numbers agree with the lower limit of 2.765 eV obtained here. Given $D(Co_2^+)$ from Table I, the calculations of Gutsev *et al.*[20] predict that reaction (4a) is exothermic by 0.63 eV when forming CoO_2 ($^2A_1$), by 0.36 eV for CoO_2 ($^4A_2$), and endothermic by 0.10 eV for CoO_2 ($^6A_1$), by 1.22 eV for the cyclic peroxo isomer, and by 1.24 eV for the bent CoOO superoxo isomer. Of these various possibilities, the formation of CoO_2 ($^6A_1$) seems most consistent with our experimental threshold of 0.41 ± 0.11 eV. Danset *et al.*[19] did not report the energetics of their calculations in sufficient detail to make a comparison. Alternatively, it is possible that the Co^+ product is formed in an excited state rather than the CoO_2 product. If the exothermicity for the formation of ground-state products as calculated by Gutsev *et al.* is correct, then formation of $Co^+(a\ ^5F)$ is exothermic by 0.20 eV and of $Co^+(b\ ^3F)$ is endothermic by 0.58 eV. The latter

threshold is potentially consistent with the experimental observations, but there is no obvious reason why the formation of $Co^+(a\,^3F)$ and $Co^+(b\,^3F)$ would exhibit distinct cross-section features. Given that Co_2^+ has a sextet ground state,[61] reaction with O_2 ($^3\Sigma_g^-$) can form both $Co^+(^3F)+CoO_2(^2A_1)$ and $Co^+(^3F)+CoO_2(^6A_1)$ in spin-conserving reactions along a quartet surface. However, the $Co^+(^3F)+CoO_2(^2A_1)$ products are most likely to evolve from a doublet intermediate (as the quartet intermediate formed by interaction of these species involves no covalent bond formation), which cannot be formed in a spin-allowed process from $Co_2^+(^6\Gamma_g)+O_2(^3\Sigma_g^-)$. Thus, reaction of $Co_2^+ + O_2$ along a quartet surface may form $Co^+(a\,^3F)+CoO_2(^6A_1)$ excited-state products easily, whereas the formation of ground-state $Co^+(a\,^3F)+CoO_2(^2A_1)$ products may involve a more complex coupling of surfaces having different spin. The relative magnitudes and dependence on energy of the two features in the Co^+ cross section, Fig. 1, are consistent with such a conjecture.

E. Trends in oxygenated cobalt cluster stabilities

The various cobalt cluster-oxygen bond energies derived above are shown as a function of cluster size in Fig. 8. As found previously for iron, chromium, vanadium, and nickel cluster ions,[5–8] it can be seen that the cluster-oxygen bond energies do not vary strongly with cluster size. It can also be seen that the Co_n^+-O bond energies derived from the secondary $Co_{n-1}O^+$ product thresholds agree fairly well with half the Co_n^+-2O bond energies and vary with cluster size similarly throughout most of the range investigated (n=3–17), although the Co_n^+-O bond energies are systematically lower with a difference of 0.35±0.12 eV in this range. It is possible that these slightly lower bond energies are the result of thresholds for the formation of $Co_{n-1}O^+$ shifted to higher energies by competition with the cluster-dioxide products. Alternatively, the first oxide bond energy may also reflect the need to distort the cobalt cluster to accommodate the oxygen bond. The second bond is stronger because the cluster has already paid the energetic costs of distortion. If this latter hypothesis is correct, then the bond energies for the second oxygen atom are nearly identical for different cluster sizes, averaging 5.46±0.12 eV for n=3–17. Thus the variations observed as a function of cluster size are attributable to the electronic adjustments that the cluster must make as the first cobalt oxygen bond is formed. It is also notable that the bond energies to Co_{14}^+ are noticeably stronger than to neighboring clusters, which may reflect the relative instability of Co_{14}^+.[23]

Another way to examine the trends in this thermochemistry is to compare the stabilities of bare and oxygenated cluster ions with regard to loss of a cobalt atom, the lowest-energy dissociation process in all cases. These $O_xCo_{n-1}^+-Co$ bond energies where x=1 and 2 are calculated from Eq. (24),

$$D(O_xCo_{n-1}^+ - Co) = D(Co_n^+ - xO) - D(Co_{n-1}^+ - xO) + D(Co_{n-1}^+ - Co), \quad (24)$$

where the required bond energies are taken from Tables III and V and Ref. 23. These comparisons are shown in Fig. 9. For most larger clusters ($n \geq 4$), the pattern in dissociation energies, $D(O_xCo_{n-1}^+-Co)$ is comparable to that for bare clusters, $D(Co_{n-1}^+-Co)$. The lack of large changes in the bond energies upon oxygenation simply reflects the fact that the Co_n^+-2O and Co_n^+-O bond energies do not change appreciably with cluster size, Fig. 8, except for the smallest clusters. Also note that the bond energies for Co atom loss fall well below the $D(Co_n^+-O)$ and $D(OCo_n^+-O)$ bond energies, consistent with the strong preference observed in the dissociation patterns of oxygenated cobalt cluster cations.

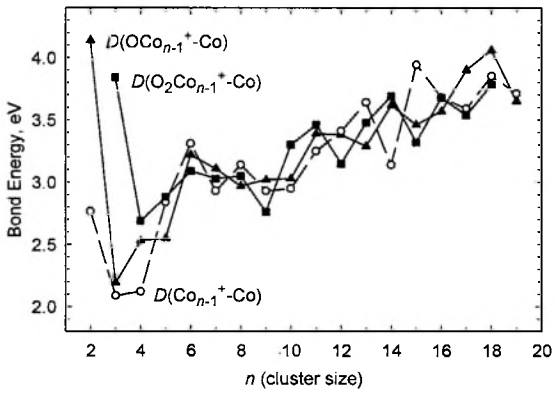

FIG. 9. Comparison of $D(O_xCo_{n-1}^+-Co)$ for x=0–2 as a function of the total number of cobalt atoms in the cluster (n). Values for x=1 and 2 are calculated using Eq. (24) and those for x=0 are taken from Ref. 23.

F. Comparison to bulk-phase thermochemistry

Having determined the bond energies for cobalt cluster oxides, we can now compare our experimental values to those obtained on bulk-phase cobalt surfaces. There have been several experimental studies on the oxidation on polycrystalline Co surfaces. Calorimetry experiments give room-temperature adsorption enthalpies for O_2 of 4.35 and 4.26 eV,[62] 4.95 eV,[63] and 4.77±0.26 eV.[64] Benziger[65] has also estimated that the atomic oxygen adsorption energy on cobalt is about 5.0 eV on the basis of enthalpies of formation of bulk compounds. These bulk-phase values are equivalent to Co_n^+-O bond energies in the range of 4.7–5.1 eV, which is comparable to half the $D(Co_n^+-2O)$ values in Table III and the $D(Co_n^+-O)$ values listed in Table V. On average, our $D(Co_n^+-2O)/2$ values equal 5.1±0.3 eV (n=4–18) and the $D(Co_n^+-O)$ values average to 4.7±0.2 (n=3–19), matching the range of bulk-phase values nicely. In addition, $\Delta_{vap}H^0$ (Co) is 4.41±0.02 eV,[66] suggesting that the metal should vaporize before oxygen desorbs for many oxidized cobalt surfaces, in agreement with the dissociation behavior observed here. Similar good agreement between cluster and bulk thermochemistry was also found in our previous studies of the oxidation of iron, chromium, vanadium, and nickel cluster ions.[5–8] This conclusion suggests that it is reasonable to use cluster models to study surface reactivities of transition metals.

One can also use the thermochemistry derived here to consider implications for various catalytic reactions. One example is Fischer-Tropsch chemistry in which CO must be dissociated (requiring 11.1 eV) and the resulting surface oxide generally removed by reactions with H_2 to form water (releasing 5.0 eV). The former reaction is clearly favored by stronger metal oxide bonds, whereas the latter needs weaker

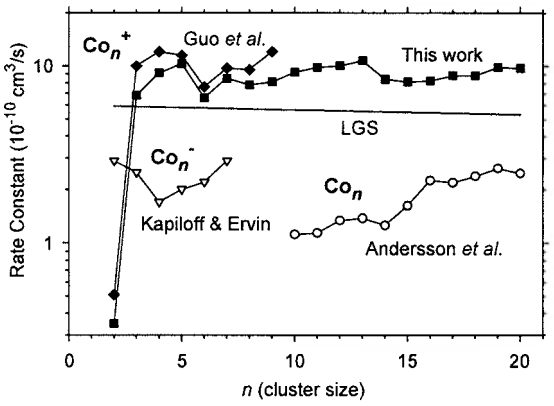

FIG. 10. Rate constants for cobalt cluster reactions with O_2. The solid symbols indicate the results for cobalt cluster cations from the present study (squares) and Ref. 13 (diamonds). The experimental values for neutral cobalt clusters are indicated by the open circles (values calculated from absolute reaction probabilities from Ref. 15, see text). The open triangles show the rate constants for cobalt cluster anions from Ref. 16. The nearly horizontal line indicates the LGS value for the collision rate constant (Ref. 55).

metal oxide bonds. The present results indicate that cobalt cluster-oxide bond energies lie close to values that enable the formation of water to be efficient, while still being as strong as possible to facilitate the CO dissociation reaction. The apparent difference in the Co_n^+–O and OCo_n^+–O bond energies may also suggest that low oxidation levels are most favorable for oxygen atom removal by H_2.

G. Reaction-rate constants

Cross sections can be converted to reaction-rate constants by using the expression,

$$k(\langle E\rangle) = v\sigma(E), \tag{25}$$

where $v=(2E/\mu)^{1/2}$ and $\mu=mM/(m+M)$, the reduced mass of the reactants. The rate constants depend on the mean energy of the reactants, which includes the average thermal motion of the neutral, such that $\langle E\rangle=E+(3/2)\gamma k_B T$, where $\gamma=M/(m+M)$. At the lowest ion energies (equivalent to 298-K thermal reactivity), our absolute rate constants agree within our experimental error of 30% with the LGS value[55] of $\sim 5.6\times 10^{-10}$ cm^3 s^{-1}, which changes slightly with cluster size, except for $n=2$ and 6. On average, these experimental rate constants are $(1.1\pm 0.2)k_{LGS}$ for $n=3$–5 and 7–20. However, if our absolute rate constants for the total reactivity of cobalt cation clusters Co_n^+ with O_2 are taken as the average over an energy range from thermal to about 0.5 eV, we obtain the values shown in Fig. 10. The rate constant for the dimer is small, over one order of magnitude lower than those for $n=3$–20. The rate constants for clusters $n=4,5,7$–20 average about 1.6 ± 0.2 times the LGS value, whereas those for $n=3$ and 6 are close to the LGS value. Clearly, the reactivity is largely independent of cluster size for $n=9$–20. These rate constants can be directly compared with the results of Guo *et al.*,[13] who examined the size dependence of gas-phase reactions of Co_n^+ ($n=2$–9) with O_2 at thermal energies using a selected ion drift tube. Figure 10 shows that our results and those of Guo *et al.* exhibit a very similar size dependence for cobalt cations in the size range of 2–9. In addition, the absolute rate constants obtained here are in good agreement with those of Guo *et al.* with our values averaging $20\pm 10\%$ lower than theirs, within the experimental uncertainty of either measurement. Clearly the fact that the rate constants (and cross sections) exceed the LGS prediction for slightly elevated energies is not an experimental artifact. Guo *et al.* discussed this discrepancy extensively and concluded that the simple LGS model could be imprecise because of nonisotropic polarizabilities and because the charge distribution and size of cobalt cluster ions might have an influence on the reaction-rate constants. As discussed above, this latter effect seems a plausible explanation for the relatively large reaction-rate constants found for oxidation of cobalt cluster cations, but these other factors could be influential as well.

Although the reaction rates of neutral, anionic, and cationic cobalt clusters with O_2 need not be similar, it is of interest to make such a comparison. Andersson *et al.*[15] have reported the absolute probabilities for reaction of neutral cobalt clusters with O_2 under near single-collision conditions. These reaction probabilities are converted to absolute rate constants by using Eq. (25) with reaction cross sections approximated by multiplying the reported reaction probabilities by the Co_n–O_2 hard-sphere cross section, $\sigma_{HS}=\pi(1.38n^{1/3}+2.325)^2$.[15] This gives rate constants for the neutral cobalt clusters ($n=10$–20), Fig. 10, that gradually increase with cluster size. Kapiloff and Ervin[16] also investigated the reactivity of cobalt anion clusters, Co_n^-($n=2$–8), toward O_2 and measured the rate coefficients using a flow tube reactor. Comparison of cationic, anionic, and neutral cobalt clusters shows that the reactivities of neutral clusters ($n=10$–20) and anionic clusters ($n=3$–7) are roughly one-third those of the corresponding cation clusters. As can be seen from Fig. 10, there is little dependence of the reaction-rate constants on cluster size for any charge state, with the notable exception of Co_2^+, although it is interesting that the reactivity of Co_4^+ is a local maximum, whereas the rate for Co_4^- is a local minimum. This suggests that the cobalt cluster-oxidation reactions are driven primarily by their exothermicities and do not exhibit a great deal of sensitivity to their geometric and electronic structures. The enhanced reactivity of the cations compared to the neutral and anionic clusters cannot be attributed to a more favorable long-range potential, as cations and anions share this property. This suggests that the electron deficient cationic clusters probably have more radical-like sites among the highest occupied orbitals, thereby driving the reactions with the biradical oxygen molecule to completion more effectively than the neutral and anionic clusters.

ACKNOWLEDGMENT

This work is supported by the Chemical Sciences, Geosciences, and Biosciences Division, Office of Basic Energy Sciences, Office of Sciences, U. S. Department of Energy.

[1] J. A. Moulijn, P. W. N. M. v. Leeuwen, and R. A. v. Santen, *Catalysis: An Integred Approach to Homogeneous, Heterogeneius and Industrial Catalysis* (Elsevier, Amsterdam, 1993).
[2] M. A. Vannice, Catal. Rev. - Sci. Eng. **14**, 153 (1976); R. B. Anderson, *The Fischer-Tropsch Synthesis* (Academic, New York, 1984).
[3] E. Iglesia, Appl. Catal., A **161**, 59 (1997); H. Schulz, *ibid.* **186**, 3 (1999).

[4] See webpage http://www.thecdi.com/cobalt
[5] S. K. Loh, L. Lian, and P. B. Armentrout, J. Chem. Phys. **91**, 6148 (1999); J. B. Griffin and P. B. Armentrout, *ibid.* **106**, 4448 (1997).
[6] J. B. Griffin and P. B. Armentrout, J. Chem. Phys. **108**, 8062 (1998).
[7] J. Xu, M. T. Rodgers, J. B. Griffin, and P. B. Armentrout, J. Chem. Phys. **108**, 9339 (1998).
[8] D. Vardhan, R. Liyanage, and P. B. Armentrout, J. Chem. Phys. **119**, 4166 (2003).
[9] J. B. Griffin and P. B. Armentrout, J. Chem. Phys. **107**, 5345 (1997).
[10] J. B. Griffin and P. B. Armentrout, J. Chem. Phys. **108**, 8075 (1998).
[11] D. B. Jacobson and B. S. Freiser, J. Am. Chem. Soc. **108**, 27 (1986).
[12] R. B. Freas, B. I. Dunlap, B. A. Waite, and J. E. Campana, J. Chem. Phys. **86**, 1276 (1986).
[13] B. C. Guo, K. P. Kerns, and A. W. Castleman, Jr., J. Phys. Chem. **96**, 6931 (1992).
[14] D. A. Hales and P. B. Armentrout, J. Cluster Sci. **1**, 127 (1990).
[15] M. Andersson, J. L. Persson, and A. Rosén, J. Phys. Chem. **100**, 12222 (1996); J. L. Persson, M. Andersson, and A. Rosén, Z. Phys. D: At., Mol. Clusters **26**, 334 (1993).
[16] E. Kapiloff and K. M. Ervin, J. Phys. Chem. A **101**, 8460 (1997).
[17] A. Pramann, K. Koyasu, A. Nakajima, and K. Kaya, J. Phys. Chem. A **106**, 4891 (2002).
[18] G. V. Chertihin, A. Citra, L. Andrews, and C. W. Bauschlicher, Jr., J. Phys. Chem. A **101**, 8793 (1997).
[19] D. Danset and L. Manceron, J. Phys. Chem. A **107**, 11324 (2003); Phys. Chem. Chem. Phys. **7**, 583 (2005); D. Danset, M. E. Alikhani, and L. Manceron, J. Phys. Chem. A **109**, 97 (2005); **109**, 105 (2005).
[20] G. L. Gutsev, B. K. Rao, and P. Jena, J. Phys. Chem. A **104**, 11961 (2000).
[21] E. L. Uzunova, G. St. Nikolov, and H. Mikosch, J. Phys. Chem. A **106**, 4104 (2002); ChemPhysChem **5**, 192 (2004).
[22] C. W. Bauschlicher, Jr. and P. Maitre, Theor. Chim. Acta **90**, 189 (1995); G. L. Gutsev, B. K. Rao, and P. Jena, J. Phys. Chem. A **104**, 5374 (2000); Y. Nakao, K. Hirao, and T. Taketsugu, J. Chem. Phys. **114**, 7935 (2001).
[23] D. A. Hales, C. X. Su, L. Lian, and P. B. Armentrout, J. Chem. Phys. **100**, 1049 (1994).
[24] F. Liu and P. B. Armentrout, J. Chem. Phys. **122**, 194320 (2005).
[25] P. B. Armentrout, D. A. Hales, and L. Lian, in *Advances in Metal and Semiconductor Clusters*, edited by M. A. Duncan (JAI, Greenwich, 1994), Vol. 2, pp. 1–39.
[26] P. B. Armentrout, J. B. Griffin, and J. Conceição, in *Progress in Physics of Clusters*, edited by G. N. Chuev, V. D. Lakhno, and A. P. Nefedov (World Scientific, Singapore, 1999), pp. 198–225.
[27] P. B. Armentrout, Annu. Rev. Phys. Chem. **52**, 423 (2001).
[28] P. B. Armentrout, Eur. J. Mass Spectrom. **9**, 531 (2003).
[29] S. K. Loh, D. A. Hales, L. Lian, and P. B. Armentrout, J. Chem. Phys. **90**, 5466 (1989).
[30] T. G. Deitz, M. A. Duncan, D. E. Powers, and R. E. Smalley, J. Chem. Phys. **74**, 6511 (1981).
[31] S. K. Loh, D. A. Hales, and P. B. Armentrout, Chem. Phys. Lett. **129**, 527 (1986).
[32] E. Teloy and D. Gerlich, Chem. Phys. **4**, 417 (1974); D. Gerlich, Adv. Chem. Phys. **82**, 1 (1992); D. Gerlich, in *State-selected and State-to-state Ion-Molecule Reaction Dynamics*, edited by C.-Y. Ng, and M. Baer (Wiley, New York, 1992), p. 1.
[33] K. M. Ervin and P. B. Armentrout, J. Chem. Phys. **83**, 166 (1985).
[34] N. R. Daly, Rev. Sci. Instrum. **31**, 264 (1959).
[35] W. J. Chesnavich and M. T. Bowers, J. Phys. Chem. **83**, 900 (1979).
[36] P. B. Armentrout, in *Advances in Gas Phase Metal Ion Chemistry*, edited by N. G. Adams and L. M. Babcock (JAI, Greenwich, 1992), Vol. 1, p. 83.
[37] P. B. Armentrout, Int. J. Mass. Spectrom. **200**, 219 (2000).
[38] L. Lian, C. X. Su, and P. B. Armentrout, J. Chem. Phys. **97**, 4072 (1992).
[39] R. G. Gilbert and S. C. Smith, *Theory of Unimolecular and Recombination Reactions* (Blackwell Scientific, Oxford, 1990).
[40] K. A. Holbrook, M. J. Pilling, and S. H. Robertson, *Unimolecular Reactions*, 2nd ed. (Wiley, New York, 1996).
[41] D. G. Truhlar, B. C. Garrett, and S. J. Klippenstein, J. Phys. Chem. **100**, 12771 (1996).
[42] M. T. Rodgers, K. M. Ervin, and P. B. Armentrout, J. Chem. Phys. **106**, 4499 (1997).
[43] A. A. Shvartsburg, K. M. Ervin, and J. H. Frederick, J. Chem. Phys. **104**, 8458 (1996).
[44] R. J. Birgeneau, J. Cordes, G. Dolling, and A. D. Woods, Phys. Rev. **136**, 1359 (1964).
[45] G. Simmons and H. Wang, *Single Crystal Elastic Constants and Calculated Aggregate Properties: A Handbook*, 2nd ed. (MIT, Cambridge, MA, 1971).
[46] N. W. Ashcroft and N. D. Mermin, *Solid State Physics* (Saunders College, Philadelphia, 1976), p. 461.
[47] R. Röhlsberger, W. Sturhahn, T. S. Toellner, K. W. Quast, M. Hwssion, M. Hu, J. Sutter, and E. E. Alp, J. Appl. Phys. **86**, 584 (1999).
[48] E. R. Fisher, J. L. Elkind, D. E. Clemmer, R. Georgiadis, S. K. Loh, N. Aristov, L. S. Sunderlin, and P. B. Armentrout, J. Chem. Phys. **93**, 2676 (1990).
[49] See EPAPS Document No. E-JCPSA6-123-042528 for 17 figures. This document can be reached via a direct link in the online article's HTML reference section or via the the EPAPS homepage (http://www.aip.org/pubservs/epaps.html).
[50] R. H. Page and C. S. Gudeman, J. Opt. Soc. Am. B **7**, 1761 (1990).
[51] L. M. Russon, S. A. Heidecke, M. K. Birke, J. J. Conceicao, P. B. Armentrout, and M. D. Morse, Chem. Phys. Lett. **204**, 235 (1993); L. M. Russon, S. A. Heidecke, M. K. Birke, J. J. Conceicao, M. D. Morse, and P. B. Armentrout, J. Chem. Phys. **100**, 4747 (1994).
[52] E. R. Fisher and P. B. Armentrout, J. Phys. Chem. **94**, 1674 (1990).
[53] P. B. Armentrout and B. L. Kickel, in *Organometallic Ion Chemistry*, edited by B. S. Freiser (Kluwer, Dordrecht, 1996), pp. 1–45.
[54] M. W. Chase, C. A. Davies, J. R. Downey, D. J. Frurip, R. A. McDonald, and A. N. Syverud, J. Phys. Chem. Ref. Data Suppl. **14**, 1 (1985).
[55] G. Gioumousis and D. P. Stevens, J. Chem. Phys. **29**, 294 (1958).
[56] E. W. Rothe and R. B. Bernstein, J. Chem. Phys. **31**, 1619 (1959).
[57] C. Rue, P. B. Armentrout, I. Kretzschmar, D. Schröder, J. N. Harvey, and H. Schwarz, J. Chem. Phys. **110**, 7858 (1999).
[58] M. F. Jarrold and J. E. Bower, J. Chem. Phys. **87**, 5728 (1987).
[59] J. B. Pedley and E. M. Marshall, J. Phys. Chem. Ref. Data **12**, 967 (1983).
[60] R. T. Grimley, R. P. Burns, and M. G. Inghram, J. Chem. Phys. **45**, 4158 (1966).
[61] G. L. Gutsev and C. W. Bauschlicher, Jr., J. Phys. Chem. A **107**, 4755 (2003).
[62] I. Toyoshima and G. A. Somorjai, Catal. Rev. - Sci. Eng. **19**, 105 (1979).
[63] C. N. R. Rao, P. V. Kamath, and S. Yashonath, Chem. Phys. Lett. **88**, 13 (1982).
[64] V. E. Ostrovskii, Russ. J. Phys. Chem. **62**, 330 (1988).
[65] J. B. Benziger, in *Metal-Surface Reaction Energetics*, edited by E. Shustorovich (VCH, New York, 1991), p. 53.
[66] M. W. Chase, Jr., C. A. Davies, J. R. Downey, Jr., D. J. Frurip, R. A. Mcdonald, and A. N. Syverud, J. Phys. Chem. Ref. Data Suppl. **17**, 1 (1988).